JOURNAL OF APPLIED ELECTROCHEMISTRY 18 (1988) 154–161

Crystal structure and morphology of electrodeposited zinc-iron binary alloys

K. KONDO, S. HINOTANI, Y. OHMORI

Technical Research Laboratories, Sumitomo Metal Industries, Ltd, 1-3, Nishinagasu-hondori, Amagasaki 660, Japan

Received 29 April 1987; revised 26 July 1987

Deposits of zinc-iron alloy have been prepared galvanostatically from a sulphate bath and the crystal structure has been determined by X-ray diffraction and transmission electron microscopy measurements. The electrodeposited zinc-iron alloys have metastable structures and the individual phases coexist over wide composition ranges. The phases are identified as η(100 ~ 73 at % zinc), Γ(87 ~ 48 at % zinc), Γ_1(78 ~ 62 at % zinc) and α(62 ~ 0 at % zinc). The c and c/a in the h.c.p. lattice of the η-phase decrease continuously with decrease of zinc concentrations, and the latter changes from 1.86 to 1.60 (a and c are the lattice constants of the η-phase in the direction of the a- and c-axes, respectively). The η-phase particles exhibit a hexagonal plate-like morphology which is thin in the direction of the c-axis. The morphology of the electrodeposits changes from plate-like to pyramidal shape when fine η-phase particles (~ 100 nm) start to form surrounding the η-phase platelets, and then to lenticular or granular in the Γ/Γ_1 duplex region. The α-phase forms in the low zinc concentration region and changes the electrodeposits to a fine cuboidal morphology.

1. Introduction

Zinc-iron electrodeposition on cold-rolled strips has been widely used in the automobile industry for the improvement of corrosion resistance and of capability for organic coating. In principal, these properties should depend on the crystal structure and the morphology of the deposits. The crystal structure determination of zinc-iron electrodeposits, however, is rather complicated because various phases such as η(hexagonal), Γ(b.c.c.), α(b.c.c.) which is the solid solution of zinc and iron, and the large unit cell phases of Γ_1(f.c.c.), δ_1, δ(hexagonal) and ζ(monoclinic) are said to form. Dalal *et al.* [1] examined electrodeposits of low zinc concentration and showed that Γ and α-phases form, while Shima *et al.* [2] reported that η and Γ-phases are deposited in the zinc-rich region, and that the ratio of the lattice constants, c/a, of the η-phase changes continuously with zinc concentration. In electrodeposits annealed at 350° C, on the other hand, the formation of Γ_1 and δ_1-phases have also been suggested [3] and further detailed study is needed to understand the zinc-iron electrodeposits comprehensively.

The inconsistencies mentioned above are probably due to the formation of metastable compounds. It should also be noted that the zinc-iron binary alloys precipitate so-called electron compounds of D-8_2 structure as in the case of Cu-Zn and Ni-Zn binary alloys and the crystal structure changes in a rather complicated way according to the valency electron to atom ratio (e/a). In the present report, the structure and morphology of zinc-iron electrodeposits have been examined with varying zinc concentration.

2. Experimental details

All plating experiments were carried out under galvanostatic control and a rotating disk electrode was used in order to control the plating conditions. The electrolyte was prepared from analytically pure reagents and de-ionized water. The bath composition and the plating condition are summarized in Table 1. Since the concentration of the Fe^{+++} ion changes quite readily, it was carefully controlled within the range of 800 ~ 1500 p.p.m. throughout the experiments. Disks of a low carbon steel sheet with a diameter of 30 mm were used as cathodes. Prior to plating, the cathodes were mechanically polished, degreased in acetone with ultrasonic cleaning, pickled with 10% sulphuric acid and rinsed in deionized water. In order to avoid the effect of non-uniformity of current density, small disks of 6 mm diameter were mechanically punched out every 6 mm from the center of the cathode and the chemical composition of the deposits were analysed (Fig. 1). Since the composition was almost uniform up to 9 mm from the centre of the cathode, all analyses were carried out within this region. The morphology of the deposits was observed by scanning electron microscopy. The X-ray diffraction technique using Co-K_α radiation operating at 30 kV and 100 mA, and transmission electron microscopy at an accelerating voltage of 200 kV were used for the examination of the structure of the crystals. The electrodeposited films used for TEM observation were removed from the titanium substrate which had been passivated in concentrated nitric acid and rinsed in deionized water prior to plating. Thin foils were prepared by means of a twin jet polishing technique

0021-891X/88 $03.00 + .12

Table 1. Bath composition and condition of electroplating

Bath composition	$FeSO_4$: 0.9 × 10^3 mol m^{-3}, Na_2SO_4: 1.2 × 10^3 mol m^{-3} $ZnSO_4$: 0.17, 0.35, 0.52, 0.73, 0.87, 1.0 × 10^3 mol m^{-3}
Condition of plating	Fe^{+++}: 500–1500 p.p.m. pH: 1.5 bath temperature: 50° C current, time: 8000 A m^{-2}, 10 sec

in mixed electrolyte solution of either acetic and perchloric acids for the iron rich specimens or sodium rhodanid and 2-n butoxyethanol for the zinc-rich specimens. For chemical analysis, the deposits on the steel were dissolved in 10% hydrochloric acid solution.

3. Results

3.1. *X-ray diffraction*

Since the results of X-ray diffraction of zinc-iron deposits cannot be determined straightforwardly, the relationships between the interplanar-spacings and the chemical compositions of the deposits are shown in Fig. 2. The interplanar-spacings vary continuously with the compositions of the deposits and can be divided into three groups by their compositions. They can be identified as η, Γ and α-phases, if the gradual change of the interplanar-spacings do not reflect the structural change. Following this interpretation η, Γ and α-phases are thought to form in the regions of 73 to 100, 48 to 87 and 0 to 62 at % of zinc, respectively. It should be kept in mind that since the reflections from $\{410\}_\Gamma$, $\{322\}_\Gamma$ and $\{331\}_\Gamma$ are forbidden in the case of b.c.c. structure, these should be indexed as $\{820\}_{\Gamma_1}$, $\{644\}_{\Gamma_1}$ and $\{662\}_{\Gamma_1}$ of f.c.c. structure. Details will be discussed in the next section.

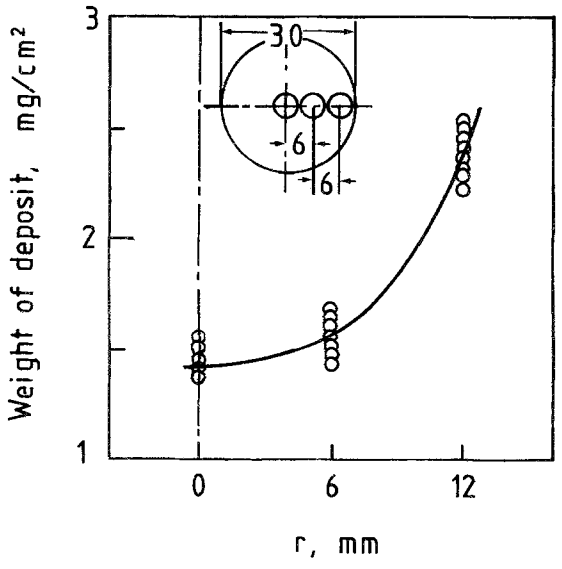

Fig. 1. Variation of the local weight/unit area of zinc-iron deposit with the distance from the center of the cathode disk. Length units are mm.

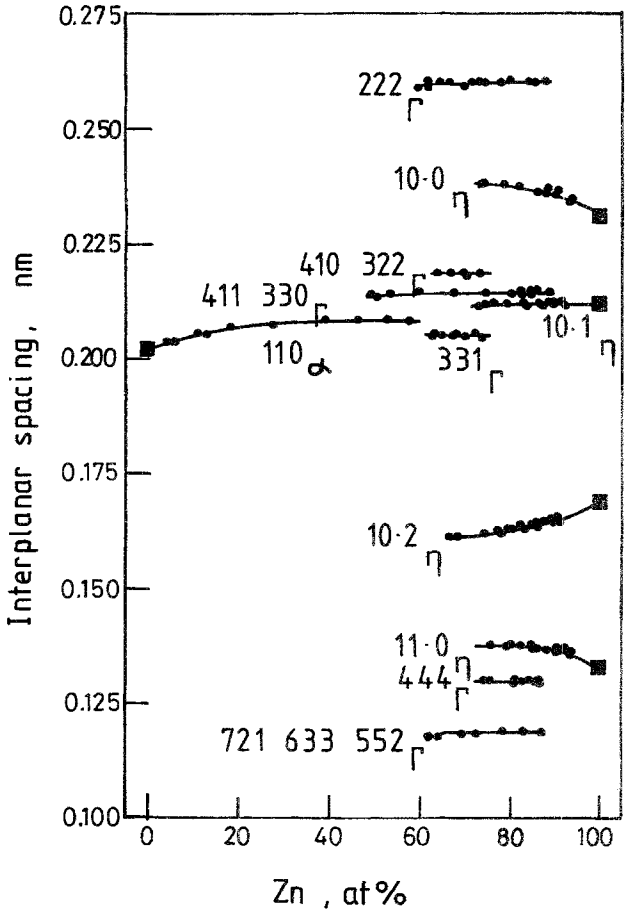

Fig. 2. Interplanar-spacings obtained by X-ray diffraction for the zinc-iron deposits. (■) Interplanar-spacings for pure zinc and pure iron; (●) Observed interplanar-spacings.

Fig. 3 shows typical profiles of X-ray diffraction from the deposits. The reflections from $\{10.0\}_\eta$, $\{10.1\}_\eta$ and $\{11.0\}_\eta$ are relatively sharp but the half width of the $\{10.2\}_\eta$ reflection is broad. For the phase which can be indexed as Γ-phase, the intensity of the reflections from the $\{330\}_\Gamma$ and $\{411\}_\Gamma$ planes is quite strong and the other reflections such as $\{222\}_\Gamma$ are rather vague.

Fig. 4 shows the composition dependence of the interplanar-spacings which can be identified as η-phase. The interplanar-spacings of $\{10.0\}_\eta$, $\{10.1\}_\eta$ and $\{11.0\}_\eta$ decrease, but that of $\{10.2\}_\eta$ increases with increasing zinc-iron ratio. Each interplanar-spacing extrapolated to pure zinc is in good agreement with that of the η-phase. The variation of the lattice constants (a and c) of the η-phase with composition was calculated. Although the lattice constants in the direction of the a-axis calculated using $\{10.0\}_\eta$ interplanar-spacings agree exactly with those obtained by $\{11.0\}_\eta$, the lattice constants along the c-axis calculated from $\{10.0\}_\eta$ and $\{10.1\}_\eta$ interplanar-spacings always show slightly larger values than those obtained from $\{10.0\}_\eta$ and $\{10.2\}_\eta$ interplanar-spacings, as in Fig. 5. The marked increase of the lattice constant in the c-axis in the zinc concentration range above 85 at % causes a large change in c/a ratio from 1.60 to 1.86.

Fig. 6 shows the interplanar-spacings and the calculated lattice constants of the Γ-phase at various zinc concentrations. The lattice constant increases slightly

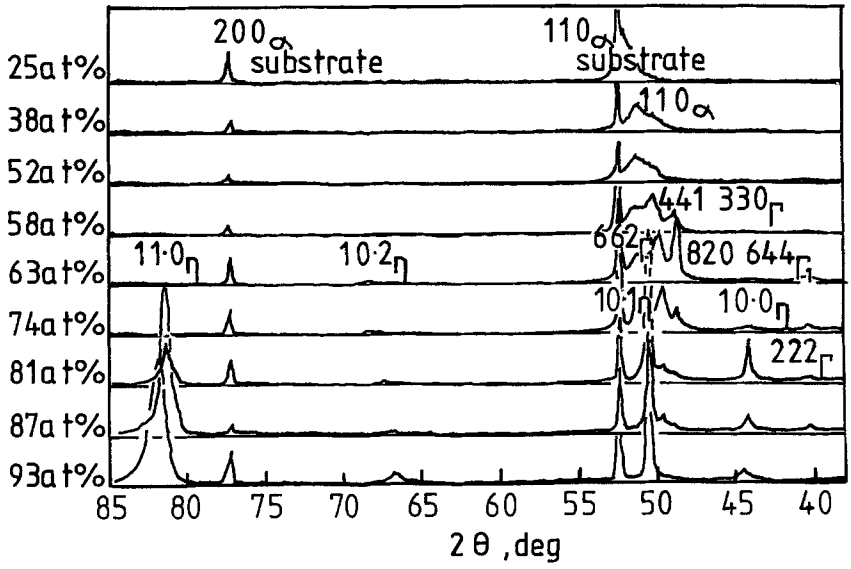

Fig. 3. X-ray diffraction profiles from the zinc-iron deposits with various zinc contents (2θ = 38 ~ 85°).

in the region of 50 to 60 at % zinc but further increase of zinc does not affect the lattice constant.

3.2. *Transmission electron microscopy*

In order to confirm the results obtained by X-ray diffraction, the zinc-iron electrodeposited films were also examined by means of transmission electron microscopy using the selected area electron diffraction technique. Fig. 7 shows the microstructure and the diffraction pattern obtained from an electrodeposited film containing 96 at % zinc. The bright and dark field images show that the deposited particles are relatively coarse, the mean linear intercept being 1 μm (Fig. 7a, b). These particles can be identified as η-phase by the diffraction pattern (c, d). In the 80 at % zinc electrodeposited film, the structure comprises η and Γ-phases (Figs 8a ~ d). Fig. 8(b) is the dark field image using the $\{\bar{1}1{\cdot}\bar{1}\}_\eta$ reflection and (d) is obtained by using a part of the $\{411\}_\Gamma$ and $\{330\}_\Gamma$ reflecting ring. Γ-phase particles are very small in size (about 100 nm) and are dispersed between the surrounding coarse η-phase particles. The deposited particles in the 67 at % zinc film are much finer as can be seen in Figs 9(a) and (b), and are almost randomly oriented as can be seen in the diffraction pattern (Fig. 9c). The close examination of this pattern (Fig. 9c) compared with that of 80 at % diffraction rings from the Γ-phase particles in Fig. 8(c) reveals that, although the reflections from the planes

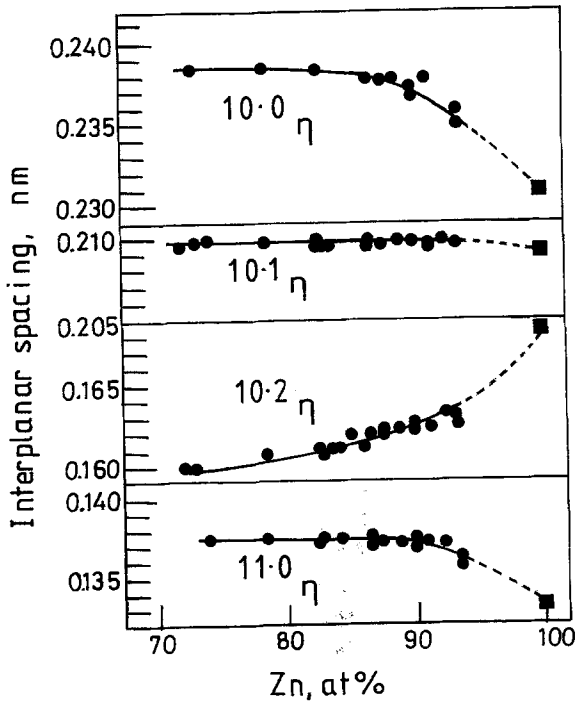

Fig. 4. Observed interplanar-spacings for η-phase. (■) Interplanar-spacings for pure zinc; (●) Observed interplanar-spacings.

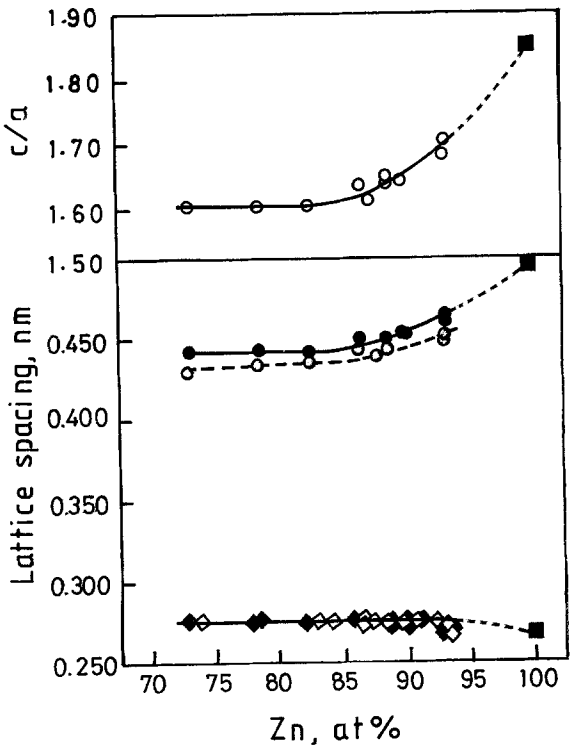

Fig. 5. Lattice spacings and c/a ratios of η-phase calculated by the data shown in Fig. 4. (■) Lattice spacing and c/a ratio for pure zinc; (○) Observed c/a ratio; (● ◒) Lattice spacing in the direction of c-axis calculated by $d_{10.0_\eta}$, $d_{10.1_\eta}$ and $d_{10.0_\eta}$, $d_{10.2_\eta}$, respectively, (◆ ◇) Lattice spacing in the direction of a-axis calculated by $d_{10.0_\eta}$ and $d_{11.0_\eta}$, respectively.

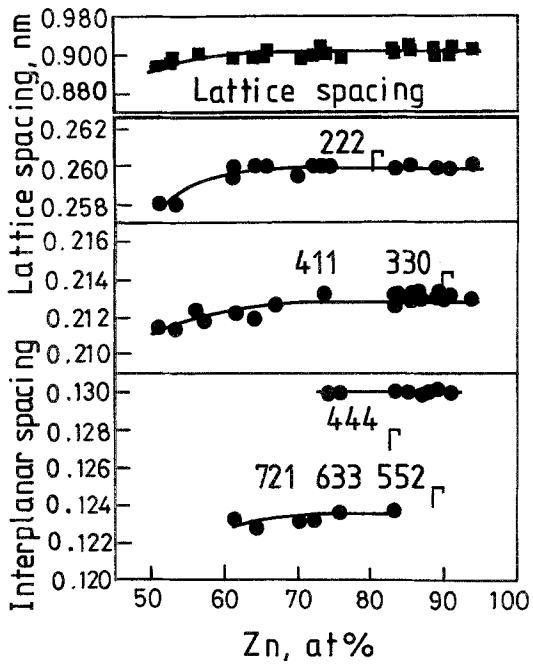

Fig. 6. Observed interplanar-spacings and calculated lattice spacing for Γ-phase. (■) Lattice spacing; (●) Interplanar-spacing.

with the interplanar-spacing of about 0.215 nm exhibit a specific distance from the electron beam center in the case of 80 at % zinc, those in 67 at % zinc film split into three different distances (Fig. 10). This suggests that the deposit of 67 at % zinc consists of both Γ and Γ_1-phases as has been demonstrated in the X-ray diffraction results. The interplanar-spacings obtained by selected area electron diffraction for both cases are summarized in Table 2. These results also confirm the above mentioned interpretation.

3.3. *Scanning electron microscopy*

Typical morphologies of zinc-iron deposits are summarized in Fig. 11. Although the deposits exhibit various shapes with change in electroplating condition, the morphology is basically determined by both the structure of the crystals and the zinc-iron ratio with the present experiments. The hexagonal thin plates of the η-phase form in the zinc concentration range above 87 at % zinc. In the η/Γ two phase region, containing 73 to 87 at % zinc, η-plates increase in thickness and become of pyramidal shape as far as SEM observation is concerned. Therefore the fine Γ particles observed by TEM are thought to disperse between these coarse η particles. Further decrease of zinc concentration reduces the coarse η-particle formation and induces Γ_1-phase particles in addition to Γ-phase. The shape of these deposits are either lenticular or granular and their grain size becomes smaller. In the range of zinc concentration below 62 at % where the α-phase forms, the deposits consist of quite fine cuboidal particles.

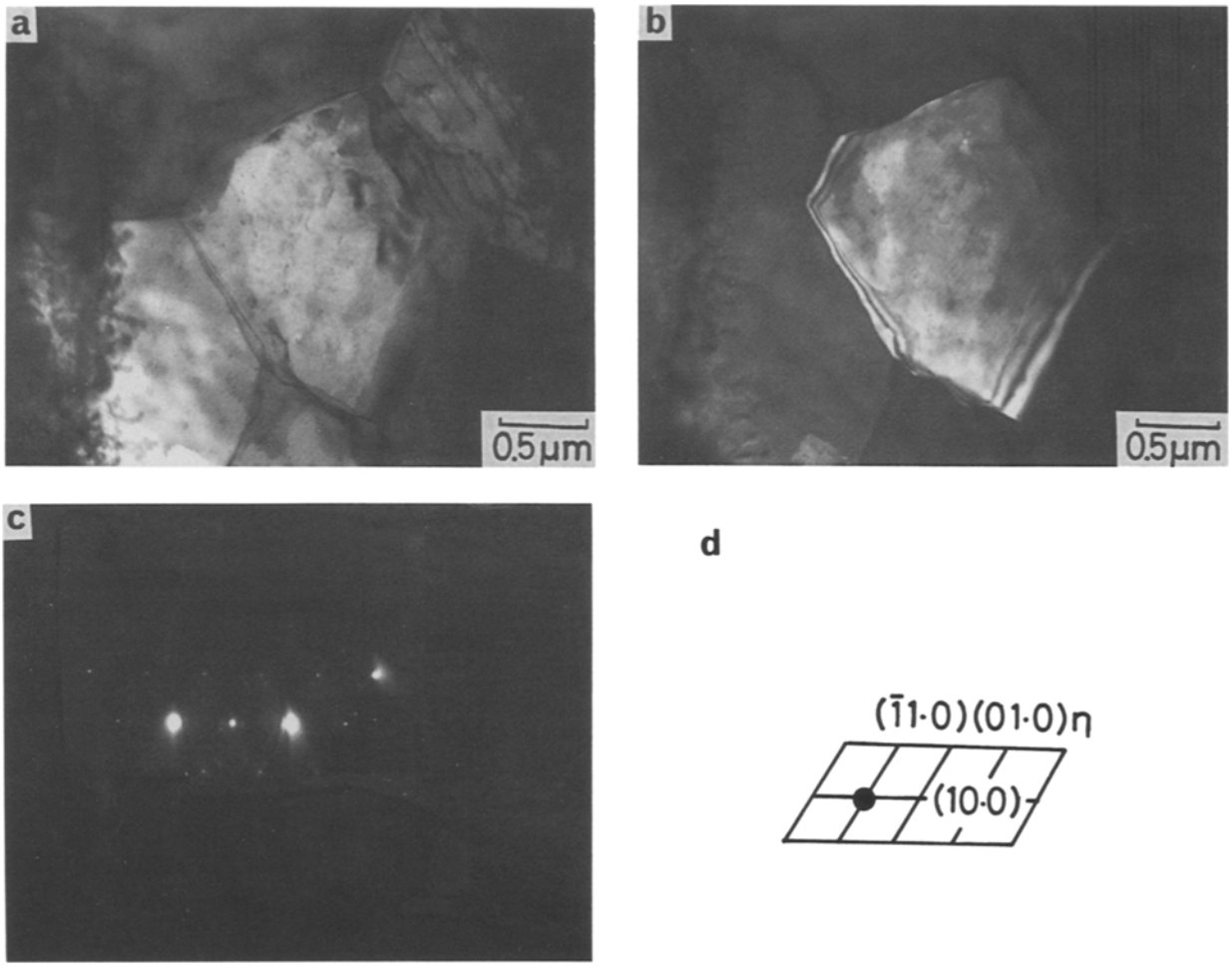

Fig. 7. Transmission electron micrographs of the electrodeposited film of 86 at % zinc. (a) Bright field image; (b) Dark field image using the $(10.0)_\eta$ reflection; (c) Diffraction pattern; (d) Schematic illustration of the pattern.

Table 2. Interplanar-spacings obtained for Γ-phase containing 80 at % zinc and Γ/Γ$_1$ duplex phase containing at % zinc

80 at % Zn	Γ(b.c.c.)		67 at % Zn	Γ_1(f.c.c.)	
d_{obs}, nm	d_{cal}, nm	h.k.l.	d_{obs}, nm	d_{cal}, nm	h.k.l.
–	–	–	0.403	0.4020	420
0.366	0.3666	211	–	0.3671	422
0.260	0.2592	222	0.262	0.2593	444
–	0.2401	321	0.240	0.2401	642
–	–	–	0.217	0.2178	820,644
0.212	0.2116	330,411	0.213	0.2117	660,822
–	–	–	0.207	0.2074	751,555
–	0.1915	332	0.192	0.1915	664
–	–	–	0.162	0.1620	1111,775
–	0.1540	530,433	0.154	0.1540	1060,866
0.150	0.1497	600,442	–	0.1497	1200,884
–	0.1354	622	0.136	0.1354	1244
0.129	0.1295	444	0.131	0.1296	888
–	–	–	0.124	0.1237	1193,997
–	–	–	0.120	0.1190	1444,1088
–	0.11407	651,732	0.115	0.1141	12 102,1464
–	0.11056	811,741	0.112	0.1106	1622,1482,10 108
0.110	0.111	811,741	–	0.11056	1622,1482,10 108
–	0.1070	653	0.107	0.1075	12 106
0.105	0.1058	660,822	–	0.1059	12 120, 1644

4. Discussion

The deposits containing zinc above 87 at % exhibit hexagonal structure and the c/a ratio changes from 1.60 to 1.86 with increasing zinc concentration. The c/a ratio extrapolated to pure zinc agrees well with that of the η-phase. In general the close-packed hexagonal electron compound, i.e. $a/c \sim 1.6$, is called ε-phase [4] and is thought to be completely different from η-phase. In the present case, however, it seems

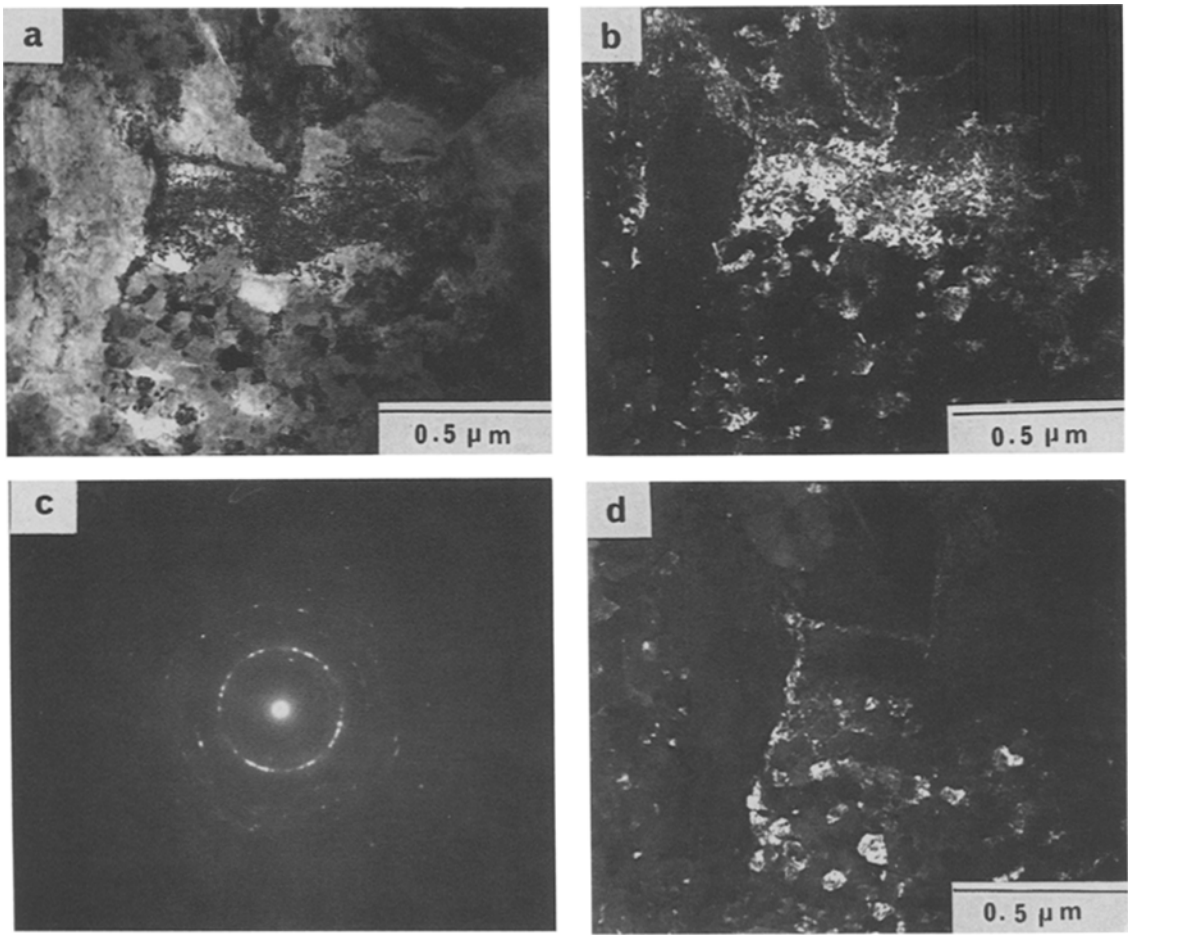

Fig. 8. Transmission electron micrographs of the electrodeposited film of 80 at % zinc. (a) Bright field image; (b) Dark field image using the $(\bar{1}1.\bar{1})_\eta$ reflection; (c) Diffraction pattern from Γ-phase region; (d) Dark field image using the $(330)_\Gamma$, $(411)_\Gamma$ reflection.

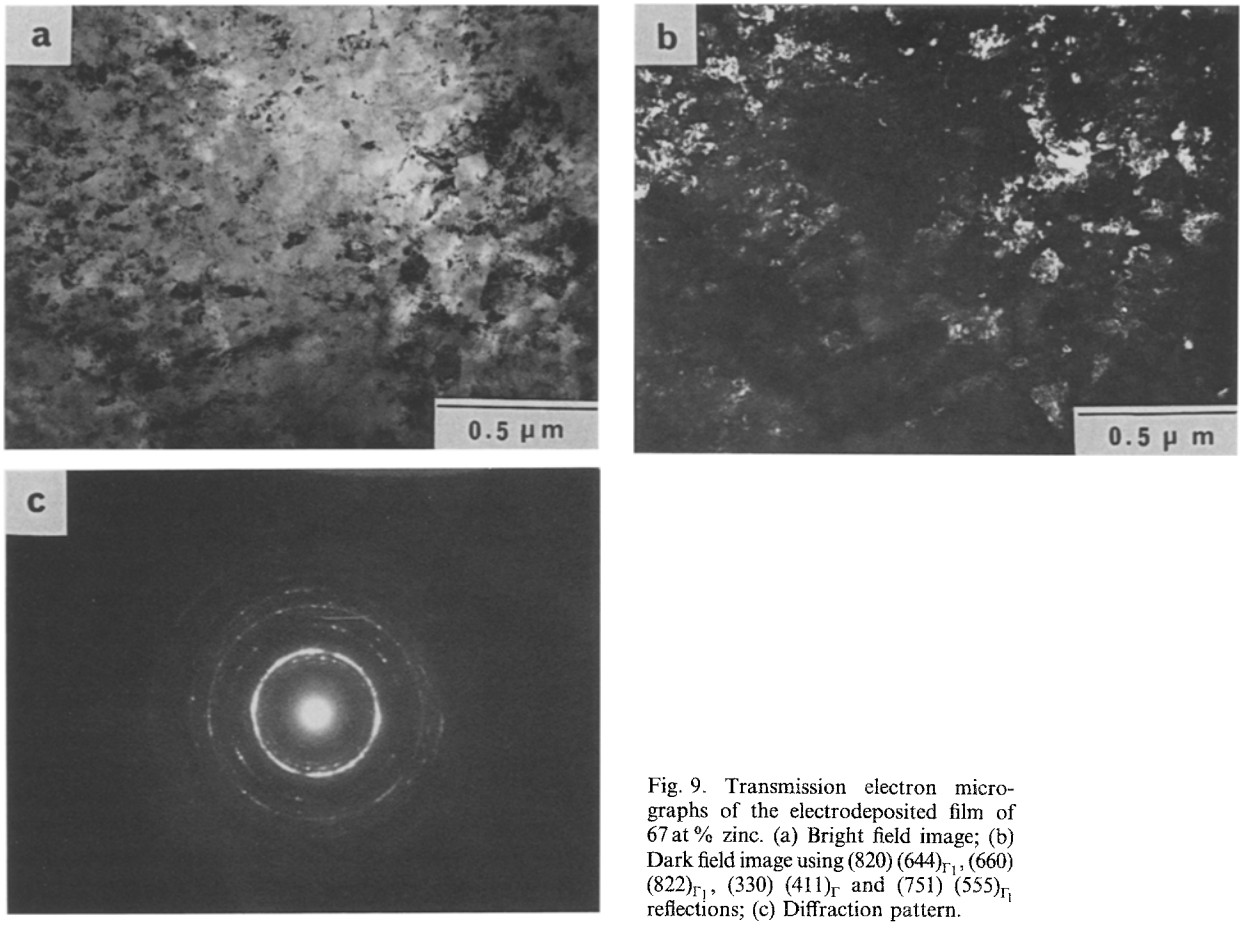

Fig. 9. Transmission electron micrographs of the electrodeposited film of 67 at % zinc. (a) Bright field image; (b) Dark field image using (820) $(644)_{\Gamma_1}$, (660) $(822)_{\Gamma_1}$, (330) $(411)_{\Gamma}$ and (751) $(555)_{\Gamma_1}$ reflections; (c) Diffraction pattern.

reasonable to classify the deposits as η-phase as has been suggested by Shima *et al.* [2], since the variation of c/a ratio with zinc concentration is continuous. It should also be noted that the angular spread of the $\{10.2\}_\eta$ reflection is much broader than that of the $\{10.1\}_\eta$, and that the reflecting angle of the $\{10.2\}_\eta$ is slightly shifted. Such a shift is often observed in the case of the hexagonal lattice containing stacking faults [5]. Although stacking faults were difficult to observe by means of transmission electron microscopy because of the high dislocation density, the existence of instrinsic stacking faults is expected since the $\{10.2\}_\eta$ is a twinning plane and the lattice constant in the direction of the c-axis calculated from $d_{10.0_\eta}$ and $d_{10.2_\eta}$ is always smaller than that from $d_{10.0_\eta}$ and $d_{10.1_\eta}$ (Fig. 5).

The Γ/Γ_1 duplex phase forms in the zinc concentration range of 48 to 87 at %. The Γ-phase in the zinc-iron system has the b.c.c. structure ($D8_2$-type) similar to γ-brass [6]. The formation of this structure is quite reasonable, since the first Jones zone of the γ-brass-type structure is a polyhedron surrounded by the planes {330} and {411} and is filled by the electrons at the valence electron to atom ratio of 1.615. In fact, very strong reflections from {330} {441} are seen in Fig. 8 as can be expected from the structure factor calculation. In the zinc concentration range of 63 to 74 at %, the reflections corresponding to the

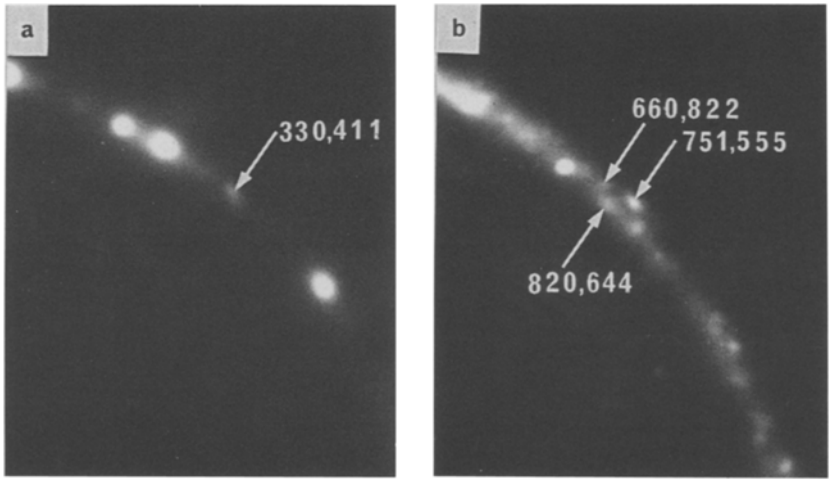

Fig. 10. A part of diffraction pattern for the interplanar-spacings in the vicinity of 0.21 nm. (a) 80 at % zinc; (b) 67 at % zinc.

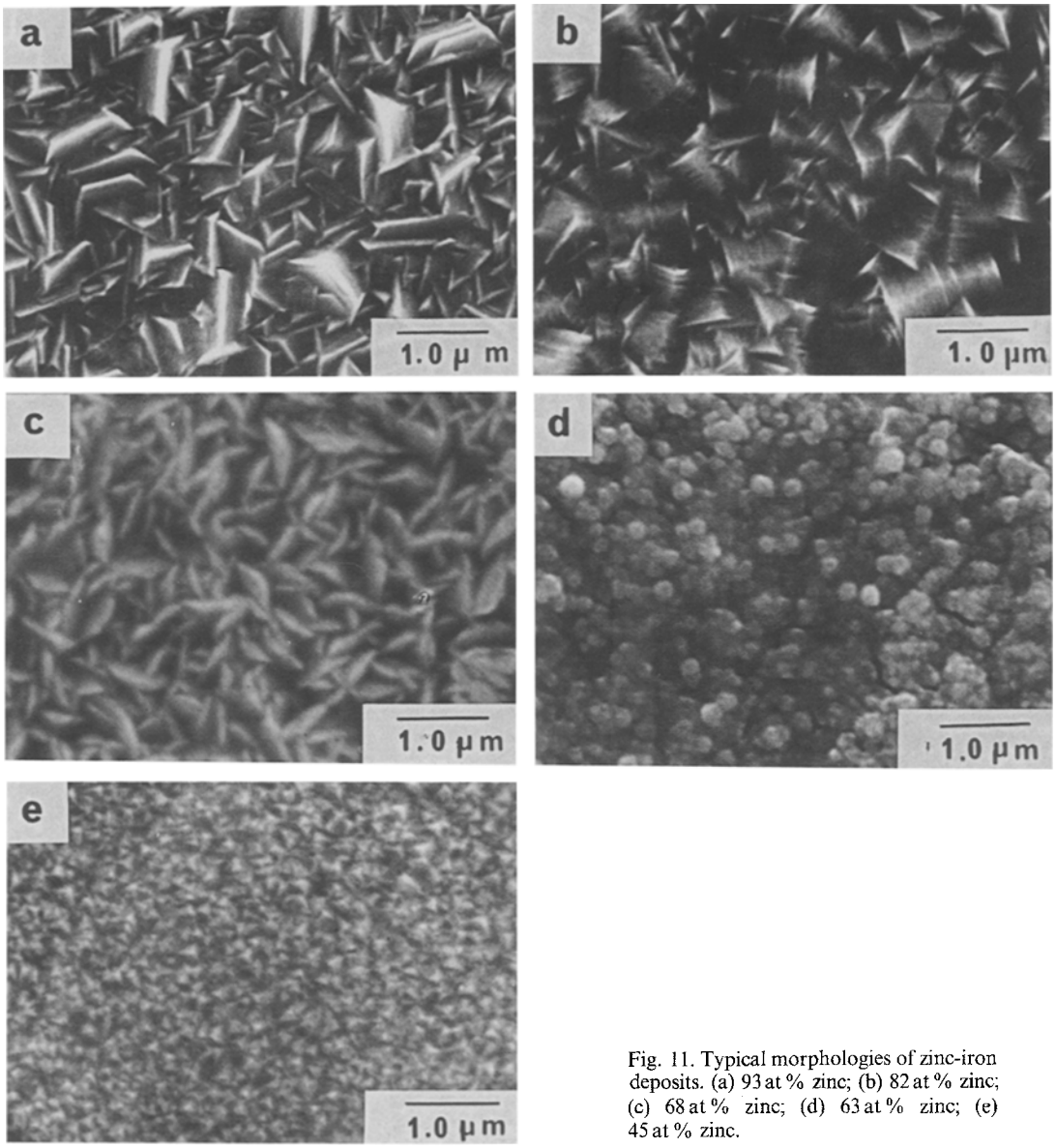

Fig. 11. Typical morphologies of zinc-iron deposits. (a) 93 at % zinc; (b) 82 at % zinc; (c) 68 at % zinc; (d) 63 at % zinc; (e) 45 at % zinc.

interplanar-spacings of 0.2174 and 0.2068 nm appear very strongly. These reflections are prohibited in the case of the Γ-phase and can only be explained by the Γ_1-phase of the f.c.c. structure of which the formation was originally confirmed by Bastin *et al.* [7], the reflections being indexed as {820} {644} (0.2178 nm) and {751} {555} (0.2074 nm) respectively (In the present work, the reflections observed can be explained consistently in terms of Γ_1-phase, but it may also be identified as δ_1-phase). Therefore it is reasonable to conclude that the Γ_1-phase forms in the range of 63 to 74 at % zinc in addition to the Γ-phase. Since the Γ-phase exists in the much broader concentration range of 38 to 87 at % zinc, the Γ_1-phase forms within this range.

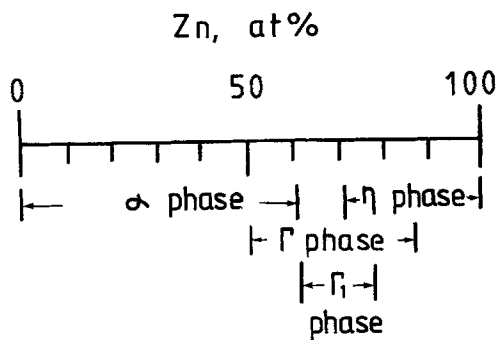

Fig. 12. Relationships between phase and composition of zinc-iron deposits.

The broad reflection in the vicinity of the $\{110\}_\alpha$ of the ferrite substrate in the low zinc concentration range (Fig. 3) deviates gradually from the $\{110\}_\alpha$ substrate reflection as zinc concentration increases (Fig. 2). This reflection can be interpreted as that from the α-phase deposit which is the solid solution of zinc and iron in keeping with the phase diagram of the binary alloy [8]. Based on the above discussion, the concentration range where various structures form in the electrodeposited zinc-iron film is schematically shown in Fig. 12.

5. Conclusions

(1) The electrodeposited zinc-iron film has metastable structures, and the individual phases have broad

co-existing concentration ranges. The phases confirmed are η(100 ~ 73 at % zinc), Γ(87 ~ 48 at % zinc), Γ_1(78 ~ 62 at % zinc) and α(62 ~ 0 at % zinc).

(2) The lattice constant in the direction of the c-axis and the c/a ratio of the η-phase decrease continuously with decrease of zinc concentration, and the latter changes from 1.86 to 1.60. Stacking faults probably exist on $\{10.2\}_\eta$ planes. Such η-phase particles exhibit a hexagonal plate-like morphology which is thin in the direction of the c-axis.

(3) The morphology of electrodeposits changes from plate-like to pyramidal shape when the Γ-phase starts to form within the η-phase, and then to lenticular or granular in the Γ/Γ_1 duplex region.

(4) In the η/Γ two phase region, Γ-phase particles are as small as about 100 nm in diameter and disperse either between coarse η-phase particles or as groups.

(5) The α-phase forms in the low zinc concentration region and exhibits fine cuboidal morphology.

(6) The crystal structure and the morphology of the deposits are mostly determined by zinc concentration within the range of the present experiments.

Acknowledgements

The authors would like to thank Dr Y. Itoh, General Manager and Director of Technical Research Laboratories; Dr T. Yukitoshi, Director of Iron & Steel Research Center, Sumitomo Metal Industries, Ltd, for permission to publish this paper. The technical assistance of Mr K. Hanafusa and Mr S. Uenoya is also appreciated.

References

[1] H. M. Dalal and D. S. Gill, *J. Inst. Metals* **93** (1964) 130.
[2] Y. Shima, S. Terasaka, K. Nakaoka, T. Hara and T. Honma, *Tetsu to Hagane* **8** (1986) 954.
[3] M. Kimoto, S. Wakano and A. Shibuya, *ibid.* **8** (1986) 961.
[4] P. Haasen, 'Physikalische Metallkunde', Ch. 6, Springer-Verlag, Berlin/Heidelberg (1974).
[5] R. Sato, *Acta Cryst.* **A25** (1969) 309.
[6] N. F. Mott and H. Jones, 'The Theory of the Properties of Metals and Alloys', Dover Publications Inc., New York (1936) p. 168.
[7] G. F. Bastin, F. J. J. van Loo and G. D. Rieck, *Z. Metallkd., Bd.* **65** (1974) 656.
[8] M. Hansen, 'Constitution of Binary Alloys', McGraw-Hill Book Co, Inc, New York, Toronto, London (1958).